Fabrication of Tissue-Engineered Tympanic Membrane Patches using 3D-Printing Technology

Elif Ilhan[1, 2], Songul Ulag[1, 3], Ali Sahin [4], Betul Karademir Yilmaz[4], Nazmi Ekren[1,5], Osman Kilic[1,6], Mustafa Sengor[1], Deepak M. Kalaskar[7], Faik Nuzhet Oktar[1, 2], Oguzhan Gunduz[1, 3*]

[1]Center for Nanotechnology & Biomaterials Application and Research (NBUAM), Marmara University, Turkey

[2]Department of Bioengineering, Faculty of Engineering, Marmara University, Turkey, 38000,34722

[3]Department of Metallurgical and Materials Engineering, Faculty of Technology, Marmara University, Turkey

[4]Department of Biochemistry, School of Medicine / Genetic and Metabolic Diseases Research and Investigation Center, Marmara University, Istanbul, Turkey.

[5]Department of Electrical and Electronics Engineering, Faculty of Technology, Marmara University, Turkey

[6]Department of Electrical and Electronics Engineering, Faculty of Engineering, Marmara University, Turkey

[7]UCL Division of Surgery and Interventional Science, Royal National Orthopaedic Hospital, Brockely Hill, HA7 4LP.

*ucemogu@ucl.ac.uk

Abstract

In recent years, scaffolds produced in 3D printing technology have become more widespread tool due to providing more advantages than traditional methods in tissue engineering applications. In this research, it was aimed to produce patches for the treatment of tympanic membrane perforations

which caused significant hearing loss by using 3D printing method. Polylactic acid(PLA) scaffolds with Chitosan(CS) and Sodium Alginate(SA) added in various ratios were prepared for artificial eardrum patches. Different amounts of chitosan and sodium alginate added to PLA increased the biocompatibility of the produced scaffolds. The created patches were designed by mimicking the thickness of the natural tympanic membrane thanks to the precision provided by the 3D printed method. The produced scaffolds were analyzed separately for chemical, morphological, mechanical and biocompatibility properties. Scanning electron microscope (SEM), Fourier-transform infrared (FT-IR) spectroscopy was performed to observe the surface morphology and chemical structure of the scaffolds. Mechanical, thermal and physical properties, swelling and degradation behaviors were examined to fully analyze whole characteristic features of the samples. Cell culture study was also performed to demonstrate the biocompatibility properties of the fabricated scaffolds with human adipose tissue-derived mesenchymal stem cells (hAD-MSCs). 15 wt % PLA was selected as the control group and among all concentrations of CS and SA, groups containing 3 wt% CS and 3 wt% SA showed significantly superior and favorable features in printing quality. The research continued with these two scaffolds (3 wt% CS, and 3 wt% SA), which showed improved print quality when added to PLA. Overall, these results show that PLA / CS and PLA / SA 3D printed artificial patches have the potential to tissue engineering solutions to repair tympanic membrane perforation for people with hearing loss.

Keywords: 3D printing, Biomaterials, Tissue Engineering, Tympanic Membrane, Artificial Eardrum Patch.

1.Introduction

The eardrum or tympanic membrane (TM) is located between the middle ear and the outer ear canal has a multi-layered structure that is less than 100 μm thickness. The eardrum has both hearing-related tasks and acts as a barrier. It captures and directs sound waves to the ossicular chain. The energy of the sound waves to the ossicles in the middle ear and then the sound waves are transferred to the inner ear(Kuypers et al., 2006). The tympanic membrane is comprised of two parts: pars flaccida(PF) containing three layers and pars tensa(PT) containing five layers where lots of perforations occur(Villar-Fernandez and Lopez-Escamez, 2015). Eardrum perforation is a widespread clinical problem in otology. The TM perforation is generally caused by trauma to the middle ear, usually, presenting with hearing loss and chronic infections(Gladstone et al., 1995). Another common cause for TM perforations is chronic otitis media (COM) and in both cases, hearing loss occurs due to ineffective sound conduction(D. et al., 2012). TM perforations are classified as acute and chronic (more than 3 months) according to their duration or wet and dry according to the presence of drainage(Villar-Fernandez and Lopez-Escamez, 2015). The healing time and closure rate also vary depending on the type of perforation. Approximately 74% of wet and acute perforations heal up to several weeks with antibiotic therapy(Zhang and Lou, 2012). While some TM perforations show spontaneous healing, especially closure of chronic perforations needs surgical intervention (myringoplasty)(Hong et al., 2013; Laidlaw et al., 2001). Two therapeutic procedures, myringoplasty, and tympanoplasty are currently performed to close TM perforations and restore function. While these surgeries performed under general and local anesthesia carry various complications and infection risks, in some cases more than one operation may be needed to close TM holes. Therefore, safer alternatives are needed for TM perforations(Teh et al., 2012). As a result in the case of chronic and non-healing perforations caused by illness, accidental trauma or certain surgical procedures, an artificial TM is required(Ghassemifar et al., 2010).

In the last century, metals, ceramics, and polymers have been used as biomaterials in surgical applications. Especially polymers have become increasingly popular in tissue engineering applications because of their biodegradability, ease of processability, and applicability(Savioli Lopes et al., 2012). Natural and synthetic polymers are particularly suitable materials for medical models and biodegradable scaffolds(Yan et al., 2018). PLA synthetic polymers with many attractive properties such as biocompatibility, high strength, stiffness hardness, thermoplasticity(Elsawy et al., 2017). It is a thermoplastic aliphatic polyester produced from agricultural products such as corn, beet(Matos et al., 2019). It is a biodegradable material used in many applications such as agriculture, medicine, and packaging(Jia et al., 2017). These properties make PLA a unique polymer for use in biomedical applications, especially in tissue engineering studies. Kozin et. al study produced a 3D printed tympanic membrane scaffold using different synthetic polymers (PLA, PCL (Polycaprolactone), PDMS (Polydimethylsiloxane)) and showed that the mechanical properties required for the tympanic membrane provided PLA with high resistance to stress(Kozin et al., 2016).

Chitosan, a dominant component of the exoskeleton of crustaceans, is a natural polymer of chitin origin. Chitosan has been shown to increase tissue formation due to mitogenic activity in biomaterial applications(Hong et al., 2013). Chitosan is a suitable candidate in tissue engineering applications because of its cell compatibility, biodegradability, flexibility, ease of formation, antimicrobial activity, and non-toxic properties(Akmammedov et al., 2017; Jayakumar et al., 2010). Patch et. al study has been reported that the eardrum patch produced using chitosan to have good biocompatibility, biodegradability, and non-toxic properties(Patch et al., 2010).

Alginate, an organic polymer usually derived from seaweed, is an excellent scaffold material for cellular growth. Alginate reduces the healing time and promotes epithelial growth,

especially in the treatment of chronic wounds. It is successfully used as a cell delivery tool for tissue regeneration. Weber et al. study compared the calcium alginate graft material with paper patch technique on chinchillas in chronic TM perforations. Alginate patches were reported to be a safe, fast, and effective way to repair small and medium-sized TM perforations. The alginate scaffold promotes cellular growth and matrix formation(Weber et al., 2006).

The main purpose of tissue engineering is to save lives and improve the quality of life. In tissue engineering, especially the repair of damaged tissues by applying the principles of biology and engineering has been studied. Scaffolds produced for tissue engineering are important materials to provide physical support to the tissue and provide cell interaction. They also function as a means of distribution to incorporate the necessary growth factors to increase tissue growth(Derakhshanfar et al., 2018). In tissue engineering, traditional methods such as electrospinning, phase separation, gas foaming, particle leaching were used to fabricate scaffolding. Although these methods have been thoroughly analyzed and optimized, there are inherent limitations(Bracaglia et al., 2017). These conventional methods can not precisely control pore geometry, pore size, and they can not create a zone of change within a single scaffold. The 3D printing method allows for overcoming these limitations by performing precise control over the design of the scaffold, unlike conventional methods. Compared to traditional tissue engineering methods, 3D printing systems have more sensibility in the spatial relationship between every element of the desired tissue(Bishop et al., 2017). 3D printing is based on the principle of layered manufacturing, in which materials are overlapped layer by layer(Yeong et al., 2006). In recent years, the development of biocompatible scaffolds with 3D printing has been particularly promising for tissue engineering applications(Gao and Cui, 2016).

In this study, it was aimed to produce biocompatible and biodegradable scaffolds which can serve as patches and repair damaged tissue for tympanic membrane perforations. In presented study, it was aimed to compare the properties of scaffolds obtained by adding two different polymers (CS and SA) onto the PLA selected as the control group. Superior properties of SA and CS compared to each other were aimed to be examined. PLA, PLA/CS, PLA/SA composite scaffolds were produced by 3D printing technology. The prepared scaffolds were investigated by using various characterization tests to examine the physical (density, viscosity, and surface tension), morphological, chemical, thermal, and mechanical properties. Furthermore, swelling and in vitro degradation behaviors, cell viability, and cell proliferation were performed to observe the biodegradation and biocompatibility properties of the fabricated scaffolds. The most significant innovation in this research compared to the previous studies about eardrum patch production techniques in the literature is that the TM patch is fabricated with 3D printing technology which can make fine adjustments on the tissue, and can produce material of the desired pore size and thickness with biocompatible and biodegradable polymers. This study contributes to the production of composite materials and fabrication of well-defined pore size and thickness required for TM patch using 3D printing process.

2.Materials and Methods

2.1.Materials

Poly (L-lactic acid) (PLA) 2003D was purchased from Nature Works LLC. Chitosan (CS, MW=50000-190000Da), Sodium alginate (SA) with an average Mn molecular weight of 216.121 g/mol and glutaraldehyde were obtained from Sigma-Aldrich. Chloroform was purchased from Sigma-Aldrich. Sodium hydroxide (NaOH), Acetic acid (CH3COOH) and Calcium chloride (CaCl2) were obtained from Yasin Teknik Company. Human adipose tissue-derived mesenchymal stem cells (hAD-MSCs) were obtained from ATCC and standard sterile cell culture techniques were used in this research for all cell seeding experiments. DMEM,

Penicillin streptomycin, and FBS were purchased from Gibco. DAPI was obtained from Thermo-Invitrogen.

2.2.Methods

2.2.1.Preparation of the Solutions

Different concentrations of PLA, PLA/CS, and PLA/SA solutions were prepared and their composition is presented in Table 1. Once dissolving PLA in Chloroform, the first scaffold candidate that will be used was obtained. 15wt.% PLA was prepared by dissolving in 10 ml chloroform at room temperature with a magnetic stirrer (WiseStir®, MSH-20A, Germany). After that, binary blends of PLA were developed using two different materials (CS, SA). PLA/CS and PLA/SA emulsion were prepared. Different amounts of CS as 1wt.%, 3wt.% and 5wt.% were dissolved in 10 ml distilled water and 0.2 ml acetic acid for 15 min. Different concentrations of SA, 1wt.%, 3wt.% and 5wt.% were dissolved in 10 ml distilled water for 20 min using a magnetic stirrer. The 5 ml solution was taken from each of CS and SA solutions and added to 10 ml 15wt.% PLA. The emulsions were stirred 1h to obtain a uniform solution. The crosslinking fluid was prepared to allow the molecules to bind together more tightly. A 5 % Sodium hydroxide solution and 1% Calcium chloride solution were used as a crosslinking agent for chitosan and sodium alginate, respectively.

2.2.2. Design and Fabrication of the 3D Printed Scaffolds

The scaffold was designed using a three-dimensional draw program (Solidworks) and converted to G-codes by Slic3r software. The scaffold configuration was designed to be a square 20 mm x 20 mm x 1 mm dimensions. The three-dimensional (3D) composite scaffolds were fabricated with an extrusion 3D printer (Hyrel 3D, SDS-5 Extruder, GA, USA). Polymer solutions were loaded into a 10 mL syringe which is directly connected to the needle with 0.2-mm diameters.3D printing was performed at a printing speed of 10 mm/s the flow rate of 1 ml/h.

The other parameters were set as follows: the infill density = 60%, the total layer = 6, and the infill pattern was rectilinear. These parameters were decided as a result of optimization studies related to 3D printer. At the end of the printing process, samples printed with pure PLA were dried to remove chloroform. Scaffolds containing chitosan were put in Sodium hydroxide solution and scaffolds containing Sodium alginate were immersed in Calcium chloride solution for 5 minutes for crosslinking. Fig. 1 briefly represented the printing process, fabrication scaffolds, eardrum patch grafting and regeneration of tissues.

2.2.3.Characterization of the physical properties of solutions

Physical analyzes of all solutions such as density, surface tension, and viscosity were performed. The density of the solutions was measured using DIN ISO 3507-Gay-Lussac (Boru Cam Inc., Republic of Turkey), a standard density bottle (10 ml). The surface tension of the solutions was calculated using a force tensiometer (Sigma 703D, Attention, Germany) at room temperature. The viscosity of the prepared solutions was measured at room temperature using a digital viscometer (DV-E, Brookfield AMETEK, USA). All equipment was calibrated before use and each test was carried out three times.

2.2.4. Fourier transform infrared spectroscopy (FT-IR)

Molecular structure and chemical characterization of scaffolds were analyzed by using Fourier transform infrared spectroscopy (FTIR, 4700 Jasco, Japan) equipped with Gladi attenuated total reflection (ATR) viewing plate (Diamond ATR crystal) and liquid-nitrogen cooled mercury cadmium telluride (MCT) detector. The results of the spectrum were analyzed at a scanning range of 450-4000 cm^{-1} and resolution of 4 cm^{-1}.

2.2.5.Scanning electron microscopy (SEM)

The surface morphology of the scaffolds was examined using scanning electron microscopy (SEM) (EVA MA 10, ZEISS, USA). Before imaging, the surface of samples was coated with gold (Au) for 120 seconds with a sputter coating machine (Quorum SC7620, ABD). Each

scaffold was analyzed about morphological properties and pore size differences. Pore sizes of scaffolds were measured using software (Analysis5, Olympus, USA) and average pore sizes were calculated for each sample.

2.2.6.Mechanical properties of the scaffolds

The tensile strength of scaffolds was determined and evaluated using a tensile test machine(SHIMADZU, EZ-LX, CHINA). Before the tensile test, the thickness of the scaffolds was measured using a digital micrometer (Mitutoyo MTI Corp., USA). All scaffolds were completely dry before the mechanical test. The upper and lower portions of each sample were located horizontally in the respective compartment of the device. Standard percentage error bars were used to obtain the standard deviation.

2.2.7.Thermal Properties of Scaffolds

The thermal characterizations such as glass transition temperatures (Tg) and melting temperature (Tm) of the 3D scaffolds were analyzed using the Differential Scanning Calorimetry (DSC) (Shimadzu, Japan). The 3D printing scaffolds were placed into aluminum pans and the temperature range was heated from 25 to 300°C at the scanning rate of 10°C/min.

2.2.8.Swelling and Degradation Behaviors of Scaffolds

The swelling and degradation properties of scaffolds were examined. The swelling test continued for one week, while the degradation test was performed for one month. The initial weights (W_0) of the scaffolds were measured on the first day. After that, all scaffolds (PLA, 15PLA/3CS, 15PLA/3SA) were placed in 2 ml phosphate buffer saline (PBS) with pH 7.4. The scaffolds were held in a thermal shaker (BIOSAN TS-100) at 37 degrees. The scaffolds were removed from PBS for day 1 after 24 hours. The excess water was absorbed and removed with filter paper. The wet weights (W_w) of the samples were measured daily (1, 2, 3, 4, 5, 6, and 7) for the swelling test. The swelling value (*S*) was calculated by using equation 1(Alhosseini et al., 2012):

$$S = \frac{(Ww - Wo)}{Wo} . 100$$ Eq (1)

The initial weights (W_0) of the scaffolds were measured on the first day. After that, all scaffolds (PLA, 15PLA/3CS, 15PLA/3SA) were placed in 2 ml phosphate buffer saline (PBS) with pH 7.4. The scaffolds were removed from PBS medium and dried at room temperature for 5 hours and they weighted (W_t) every five days (1, 5, 10, 15, 20, 25, and 30) for degradation test.

The degradation index was calculated by using equation 2(Alhosseini et al., 2012):

$$Di = \frac{(Wo - Wt)}{Wo} . 100$$ Eq (2)

2.2.9.MTT Cytotoxicity Assay, DAPI Staining, and SEM Imaging

3D Scaffolds were firstly sterilized under UV for overnight in 96 well plates. For the optimization of 3D scaffold microenvironment, the scaffolds were incubated in growth medium (DMEM with 10% FBS and 0.1mg/ml penicillin/streptomycin) for an hour at 37°C in humid 5% CO_2 incubator (SANYO). After the incubation period in the growth medium, the scaffolds were collected and the excess medium discarded by evacuating with a micropipette. $5x10^4$ human adipose tissue-derived mesenchymal stem cells (hAD-MSCs) were seeded onto the scaffolds in the 96 well plates. At the same time, monolayer (2D) cell cultures were incubated with the same number of cells in 200 µl as a control. The cell-3D scaffolds constructs and 2D cultures were incubated at 37°C, 5% CO_2 for 7 days in a humidified incubator. The scaffold biocompatibility was studied on days 1, 4 and 7. To investigate cytotoxicity at a given time point, a cytotoxicity detection kit (MTT from Glentham Life Sciences) was used. The absorbance value of the cytotoxicity test was measured at 560 nm wavelength (690 nm as Ref. value) in ELISA reader (Perkin Elmer, Enspire). The assay was studied 3 times and the average of results was considered as the final result.

To investigate the attachment of mesenchymal stem cells (MSCs) on 3D scaffolds, DAPI staining was performed. After 1, 4 and 7 days, the growth medium was discarded, and cell-3D scaffolds were washed with PBS. Afterward, all cell-3D scaffolds were fixed by adding 4%

formaldehyde for 30 min. at room temperature. Next, cell-3D scaffolds were washed with PBS. Following, 1µg/ml DAPI was added on each sample and kept for 20 min. at room temperature to stain the nucleus of the cells. Afterward, DAPI solution was discarded and cell-3D scaffolds were placed between slide and coverslip. Scaffold visualization was acquired by an inverted fluorescence microscope (Leica).

Cellular morphology of hAD-MSC on the 3D scaffolds was evaluated by scanning electron microscope (SEM). After 1, 4 and 7 days, the growth medium was discarded, all cell-3D scaffolds were fixed with 4% glutaraldehyde and then dehydrated through serial dilutions of ethanol and dried in air. The samples were sputter-coated with gold and observed by SEM (EVO MA-10, Zeiss).

2.2.10.Statistical Analysis

Statistical analyses were successfully performed by using a single factor ANOVA followed by pore size measurement using SPSS 17.0 analysis program. Statistical significance was defined as $p < 0.05$and 0.01. All quantitative results are presented as the mean ± std.

3. Results and discussion

3.1. Optimization Process and Solution Characterization

In this study, solutions were prepared by adding Chitosan and Sodium Alginate in different ratios to defined PLA concentration (Table 1). The physical properties of the prepared solutions such as density, viscosity, and surface tension were characterized and optimized. The viscosity of the solutions used in the 3D printer method is an important parameter. If the viscosity of the solution is too low, the printed strands tend to spread and cause the strands of the first layer to join. As a result, other layers bands around. On the other hand, high viscosity solutions may possibly clog the end of the dispensing needle and disrupt the next printing process, Therefore, the viscosity of the solutions to be used must be adjusted well(You et al., 2017). The other

important parameter, the surface tension determines the shape of the drop coming out of the needle and its shape on the substrate. Surface tension values of the inks generally range from 28 to 350 mN m^{-1}(Guvendiren et al., 2016). The parameters of the physical properties of seven different solutions are given in Fig. 2(a,b,c,d,e,f). Low concentrations of Chitosan and Sodium Alginate (1 wt% CS and 1 wt% SA) reduced viscosity and density of solutions when mixed with 15 wt% PLA. The printed strands were spread so that the porous structure on the scaffold was broken. Murphy et al. study showed that rising viscosity up to a certain ratio increases printability and can maintain the form of printing by preventing the solution from spreading after printing(Murphy and Atala, 2014). High concentrations of CS and SA (5 wt% CS and 5 wt% SA) increased viscosity and density when mixed with 15 wt% PLA. For this reason, the tip of the dispensing needle clogged and disrupted the structure of the scaffold. According to the Ouyang et al. study, a very high viscosity solution causes handling, and extrusion difficulties and broken printing filaments, causing problems with printability(Ouyang et al., 2016). Finally, the optimal solution density and viscosity for the needle tip and the designed scaffold used were obtained by mixing 3 wt% CS with 15 wt% PLA (15PLA/3CS) and 3 wt% SA with 15 wt% PLA (15PLA/3SA). The study was continued with these optimized data.

3.2. Fourier transform infrared spectroscopy (FT-IR)

FTIR analysis was performed to investigate the chemical and molecular structure of the scaffolds and the graphical illustration of results is shown in Fig. 3. From Fig. 3(a) and Fig. 3(b), Characteristic bands of pure PLA were observed C=O vibration peak at 1749 cm^{-1}, which can be recognized as a backbone ester group of PLA. A band, corresponding to bending vibration of CH_3 (asymmetric) was found at 1452cm^{-1}, C–O asymmetrical stretching and CH_3 twisting at 1181 cm^{-1}, C–O–C stretching at 1080 cm^{-1}, C–CH_3 stretching at 1042 cm^{-1} and C–COO stretching peak at 867 cm^{-1} (Cesur et al., 2019; Fernández-Cervantes et al., 2019). For pure CS in Fig. 3(a), related peaks were found at 3283 cm^{-1} representing the N-H stretching,

C–H vibration at 2869 cm^{-1} and primary amide C=O stretching at 1589 cm^{-1}(Ulag et al., 2020). For pure SA in Fig. 3(b), the absorption bands around 1634 cm^{-1} attributed to stretching vibrations of the asymmetric band of the -COO- group. The stretching peak at 3244 cm^{-1} corresponds to the vibrations of the O-H group. symmetric -COO-stretching peak at 1404 cm^{-1} and C–O stretching vibrations peak at 1023 cm^{-1}(Fernández-Cervantes et al., 2019; Ilhan et al., 2020). As can be seen in Fig. 3, the characteristic peaks of PLA, CS, and SA are found in the produced 15PLA/3CS and 15PLA/3SA scaffolds, respectively. The peaks of pure PLA were more dominant than CS and SA. This is due to the higher amount of PLA in two different solutions prepared with CS and SA.

3.3. SEM morphological and pore size analysis

The pore size of 3D printing scaffolds has direct implications on their functionality during tissue engineering applications. Open porous and interconnected networks are essential for tissue formation because of cell nutrition, migration, proliferation, and permeability(Loh and Choong, 2013). A porous surface also provides mechanical stability of the implant between the scaffolds and surrounding tissue(Karageorgiou and Kaplan, 2005). Besides, the structure of the pores helps promote the formation of new tissue and ensures the efficient release of biofactors and provides good substrates for nutrient exchange(Chevalier et al., 2008; Loh and Choong, 2013). Results indicated that average pore size distributions of pure PLA scaffold resulted in 155.24 µm. After the addition of the Chitosan and Sodium alginate, the average size of the pores has resulted in 160.44 µm and 129.43 µm respectively. Hutmacher et al. study showed that the pore sizes are required to be less than 300 µm in order to ensure sufficient permeability(Hutmacher et al., 2007). In the presented study, also the surface morphology of PLA, 15PLA/3CS, and 15PLA/3SA scaffolds were determined using SEM imaging. SEM images of each scaffold and their pore size histogram were shown in Fig. 4(a,b,c). While pure PLA had a smooth surface, micropores structures were obtained by incorporated with CS and

SA. In the CAD program, the scaffold was designed to be 20mm x 20mm x 1mm (X, Y, Z) and 60% infill density. The dimensions of the produced scaffolds were measured approximately 18mm x 18mm x 0.08mm(X, Y, Z). The shrinking in dimensions (X and Y) was due to the fact that the solution did not disperse much after printing because of using a high viscosity solution. The other reason is that the scaffold created in the software program has no external frame. The decrease in size (Z) is a desirable feature for the tympanic membrane patch as it is similar to the natural eardrum thickness. This is due to the low flow rate and the spreading of superimposed printed layers.

3.4. Tensile properties of engineered scaffolds

A uniaxial tensile test was performed on printed scaffolds to analyze the possible effect of pore sizes on mechanical properties which may determine their potential performance when they are inserted into the defect region (Jian et al., 2015). Tensile strength and elongation at break are the important factors found in tensile testing. Table 2 showed the tensile strength and elongation at break values of all scaffolds. The results indicated that the tensile strength of PLA had the maximum tensile strength (14.25 MPa) and strain values (6.41 %) compared to others. By adding the same amount of CS and SA into pristine PLA separately, the tensile strength values of PLA reduced to 4.72 MPa, 3.51 MPa, respectively. The reason for the decrease in mechanical properties compared to pure PLA scaffold is that chitosan and sodium alginate are natural polymers with micropores and their mechanical properties are very low. A similar decreasing pattern was numerically observed for the strain values of the scaffolds such that the percentage elongation at break of the PLA scaffold decreased sharply as the CS and SA fillers loading. Although Chitosan has attractive biological properties, its low strength and fragile behavior limit its availability (Miles et al., 2016). When the influence of pore size on mechanical properties is examined, scaffolds with a pore size of 155.24 μm (PLA), 160.44 μm (15PLA/3CS), and 129.43 μm (15PLA/3SA) caused the significant differences for tensile

strength values of scaffolds. Even though 15PLA/3SA had the minimal pore size which means that it is denser than the others, its tensile strength was found to a minimum compared to the others. It is generally known that alginate has a lower absolute value of stress than collagen, elastin and including skin, tendon, and muscle tissues, etc (Drury et al., 2004; Yang et al., 2001). However, sodium alginate can be used as a scaffold for soft tissue formation such as the tympanic membrane.

In Kim et al. research, silk fibroin and paper patches were examined and they performed tensile test to observe and compare the mechanical properties of the patches. They proved that paper patches (12.5 MPa) had higher tensile stress value than silk fibroin patches (9.7 MPa). However they reported that silk fibroin patches were more flexible (6% elongation) than paper patches (0.2% elongation)(Kim et al., 2010). In this study, PLA had both higher tensile stress and strain values than PLA/CS and PLA/SA. Thus, it was more flexible and durable than other patches. However, other patches with lower stress values can also be acceptable as a candidate of tympanic patches compared to the mechanical characteristics of human TM. Luo et al. proved that the maximum stress values of the human TM strips were range from 1.2 MPa to 22.3 MPa depending on the radial/circumferential directions, male/female, and right/left ears(Luo et al., 2009). Therefore, the tensile test results found in this study revealed desirable properties when compare to human TM.

One of the other important factors in the eardrum patch is obtaining appropriate thickness. Too thin patches tend to fold easily and may not be comfortably integrated with the natural tympanic membrane, whereas too thick patches may not be well adapted to the concave eardrum (Kim et al., 2009). In certain areas, the human natural eardrum thickness ranges from 20 to 100 μm(Fay et al., 2005; Lim, 1995). The fabricated scaffolds were analyzed for compatibility with the natural tympanic membrane thickness. The thickness of the PLA, 15PLA/3CS, and 15PLA/3SA scaffolds were measured as 40 μm, 80 μm, 60 μm by digital micrometer, respectively. The

obtained data demonstrated that the thickness of the produced scaffolds was the same ratios as that of the natural eardrum.

3.5. Investigation of the Thermal Behaviors of Fabricated Scaffolds using DSC

PLA has either semi-crystalline or amorphous structures. Its glass transition temperature (T_g) is ~55 °C and melting temperature point (T_m) ~180° C(Hamad et al., 2015). However, these values can change depending on their structures (amorphous, semi-crystalline, highly crystalline). For instance, the melting temperature value of PLA can be between 130 and 180 °C(Henton et al., 2005). DSC curves of pure PLA and 15PLA/3CS, 15PLA/3SA composites were presented in Fig. 5. In this study, the Tg of PLA was found to be 58.79 °C which is the nearly same with the Tg value of typical PLA. The melting temperature of the PLA was found to be 153.11 °C which was similar to the study of Kamthai & Magaraphan(Kamthai and Magaraphan, 2015). By the addition of SA into the PLA(15PLA/3SA), it was observed that the T_g value of PLA increased from 58.79 °C to 62.95 °C which gave 4.16 °C difference and T_m value of PLA shifted to 153.26 °C. As CS added into PLA(15PLA/3CS), T_g value was found to be 62.85 °C and T_m value decreased to 152.95 °C. There was no significant change observed in the melting temperatures between the neat PLA and the blending composites. However, there was an observed important change in the glass transition temperatures between pure PLA and the corresponding composites. It is known that glass transition temperature is affected by several factors such as chain elasticity, intermolecular interaction, and molecular weight of the substance itself(Thomas et al., 2018).

3.6. Swelling and Degradation Behaviours of Scaffolds

The ability of swelling is an essential factor in tissue engineering scaffolds due to the promoting transportation of nutrients. Swelling ability also increases mechanical resiliency(Gao et al., 2018). As shown in Fig. 6(a), the highest swelling rate was observed on the 15PLA/3SA scaffold reaching up to 250%. Samanta at al. study demonstrated that as the amount of sodium

alginate added to the solution increased, the swelling behavior of the structure improved(Samanta and Ray, 2014). When the three scaffolds (PLA, 15PLA/3CS, and 15PLA/3SA) were compared with each other, the lowest swelling rates were found to be about 50% in pure PLA scaffolds, while a swelling ratio was noticeably enhanced with the addition of Chitosan (nearly 125%). Tighzert et al. study showed that Chitosan added to the PLA up to a certain ratio increases the swelling rate by up to approximately 400%(Tighzert et al., 2017). Degradation is an event that occurs when the structures are exposed to PBS by dissolving over time(Grover et al., 2012). The degradation profile was normalized to 100% with normalization multiplier to get the same starting point for easy comparison of all scaffolds. As shown in Fig. 6(b), within 30 days, the scaffold containing Sodium Alginate demonstrated higher degradation behavior compared to the other two (PLA and 15PLA/3CS) scaffolds due to its maximum swelling capacity. Wang et al. study demonstrated that materials that absorb more water and show good swelling properties generally degrade in a shorter time(Wang et al., 2010).

3.7. In-vitro Cytotoxicity and Cell Attachment Investigation

MTT Assay was performed on 3D printed scaffolds to observe the biocompatibility properties which are the prominent effect for tissue regeneration. Some factors such as non-toxicity, good cell adhesion, proliferation, and differentiation affecting the biocompatibility of structures need to be considered(Altun et al., 2018). Mesenchymal stem cells were used because they can easily grow and differentiate into fibroblast cells in different biomaterials(Rahman et al., 2007). MTT assay was carried out for 1, 4, and 7 days incubation to determine the human mesenchymal stem cells (MSCs) viability of scaffolds. The cell viability values of the structures were shown in Fig. 7(A). According to the MSCs viability of the initial day, the viability of all scaffolds was lower than the control group (2D cell). When the viability graphic of the samples was compared, the highest viability value (91.3%) was observed in PLA scaffold and the lowest value (79.7%) was observed in the 15PLA/3SA scaffold. For day 4, the viability values of PLA

and 15PLA/3SA scaffolds were found to be 72.4% and 61.6%, respectively. On the other hand, the viability value of 15PLA/3CS scaffold increased from 81.3% to 83%. On day 7, there was seen a significant increase in cell viability values for all three scaffolds. Cell viability in PLA, 15PLA/3SA and 15PLA/3CS samples increased to 141.9%, 187.8% and 217.8% after 7 days of incubation, respectively. Abbah et al. study observed that the number of cells encapsulated in alginate doubled from 1 day incubation to the 7. day(Abbah et al., 2006). Yaret et al. study compared the cell viability and proliferation of pure PLA with different concentrations of PLA/CS composites. It was observed that cell proliferation and adhesion increased with rising chitosan concentration in the PLA/CS composites compared to pure PLA(Torres-Hernández et al., 2018). In a similar study, the proliferation of bone marrow mesenchymal stem cells increased with higher concentration CS in PLA/CS composite(Zhang and Cui, 2012). As can be seen, the cell viability test results are similar to the biological tests performed in the literature. The fluorescence microscopy images were taken to prove the viability of the cells on the 3D printed scaffolds, as indicated in Fig. 7(B). As seen in Fig. 7(B), the density of living cells is highest in the PLA scaffold. The smooth surface of the PLA is suitable for the cell population, which starts slowly from the first day and increases with time(Torres-Hernández et al., 2018). The density of live cells was lower in the surface of 15PLA/3CS and 15PLA/3SA scaffolds. This may be due to the placement of MSCs in the microporous structures of chitosan and sodium alginate. This is because the low irradiation from the fluorescence microscope has proved that the number of living cells is high, but that the cells settle in the micropore structure of chitosan and sodium alginate and remain in other layers. As can be seen, MSCs can maintain viability on the created structures and tend to proliferate and adapt to all of 3D printed.

Furthermore, cellular behavior and cell-material interaction with the 3D printed scaffolds was determined with SEM imaging. As shown in Fig. 7(C), after 4 and 7 days of incubation, mesenchymal stem cells successfully attached to the surfaces of the scaffolds. The images

clearly indicated that MSCs demonstrated appropriate cell adhesion, proliferation and spreading at all three scaffolds. After 1 day incubation, it was observed that young MSCs had spread to scaffolds to form extensions that were considered a good sign of biocompatibility. After 4 and 7 days of incubation, MSCs were observed to form orbicular structures on the surface of all three scaffolds. As can be seen, the mesenchymal stem showed good attachment to the produced PLA, 15PLA/3CS, and 15PLA/3SA scaffolds.

Biological tests show the biocompatibility of PLA/CS composites and the results observed by MTT experiments by promoting cellular activity on the composite surface suggest that cell viability is increased(Rodríguez-Vázquez et al., 2015; Tanase and Spiridon, 2014). In a study alginate reinforced by sub-micron PLA fibers found to increase cell viability compared to pure alginate(Kosik-Kozioł et al., 2017). When cell viability, proliferation, and adhesion tests were compared with biological analysis in the literature, the results were consistent with each other.

4. Conclusion

In this study, we developed novel patches for the tympanic membrane perforations as an alternative to surgical treatment or paper patch graft technique. An artificial eardrum patch was improved using the 3D printed technology to overcome the complications of traditional surgical methods or the limitations of paper patch grafting. Polylactic acid(PLA), Chitosan(CS), and Sodium alginate(SA) have been used because of their important properties for tissue engineering applications such as biocompatibility, biodegradability. Different concentrations of CS and SA were added to the pure PLA solutions, and the best concentration for printability was determined and PLA/CS and PLA/SA scaffolds were performed successfully with 3D printing method. The mechanical properties of the scaffold containing pure PLA are observed at the maximum level but there is some decline in the mechanical strength of the scaffolds obtained by adding CS and SA. However, the tensile properties of the fabricated eardrum patches produced are similar to the natural tympanic membrane. In addition, thanks to 3D

printed technology, fabricated eardrum patches have been able to mimic the thickness of the natural tympanic membrane perfectly. After 7 days of incubation, biocompatibility ratios were found to be the desired value in all three scaffolds (PLA, 15PLA/3CS, and 15PLA/3SA) as a result of cytotoxicity tests, but 15PLA/3CS scaffold showed the highest biocompatibility value and increased the binding and proliferation of MSCs. The most unique aspect of this study is the ability to produce an artificial TM patch of the desired thickness, pore size, and surface morphology, thanks to the high sensibility and printing capability of 3D printed technology.

Acknowledgments

This study was supported by FEN-B-121218-0614 BAPKO project.

References

Abbah, S.A., Lu, W.W., Chan, D., Cheung, K.M.C., Liu, W.G., Zhao, F., Li, Z.Y., Leong, J.C.Y., Luk, K.D.K., 2006. In vitro evaluation of alginate encapsulated adipose-tissue stromal cells for use as injectable bone graft substitute. Biochem. Biophys. Res. Commun. https://doi.org/10.1016/j.bbrc.2006.06.072

Akmammedov, R., Huysal, M., Isik, S., Senel, M., 2017. Preparation and characterization of novel chitosan/zeolite scaffolds for bone tissue engineering applications. Int. J. Polym. Mater. Polym. Biomater. 67, 1–9. https://doi.org/10.1080/00914037.2017.1309539

Alhosseini, S.N., Moztarzadeh, F., Mozafari, M., Asgari, S., Dodel, M., Samadikuchaksaraei, A., Kargozar, S., Jalali, N., 2012. Synthesis and characterization of electrospun polyvinyl alcohol nanofibrous scaffolds modified by blending with chitosan for neural tissue engineering. Int. J. Nanomedicine.

Altun, E., Aydogdu, M.O., Koc, F., Crabbe-Mann, M., Brako, F., Kaur-Matharu, R., Ozen, G., Kuruca, S.E., Edirisinghe, U., Gunduz, O., Edirisinghe, M., 2018. Novel Making of Bacterial Cellulose Blended Polymeric Fiber Bandages. Macromol. Mater. Eng. 303, 1–

7. https://doi.org/10.1002/mame.201700607

Bishop, E.S., Mostafa, S., Pakvasa, M., Luu, H.H., Lee, M.J., Wolf, J.M., Ameer, G.A., He, T.C., Reid, R.R., 2017. 3-D bioprinting technologies in tissue engineering and regenerative medicine: Current and future trends. Genes Dis. 4, 185–195. https://doi.org/10.1016/j.gendis.2017.10.002

Bracaglia, L.G., Smith, B.T., Watson, E., Arumugasaamy, N., Mikos, A.G., Fisher, J.P., 2017. 3D printing for the design and fabrication of polymer-based gradient scaffolds. Acta Biomater. 56, 3–13. https://doi.org/10.1016/j.actbio.2017.03.030

Cesur, S., Oktar, F.N., Ekren, N., Kilic, O., Alkaya, D.B., Seyhan, S.A., Ege, Z.R., Lin, C.-C., Kuruca, S.E., Erdemir, G., Gunduz, O., 2019. Preparation and characterization of electrospun polylactic acid/sodium alginate/orange oyster shell composite nanofiber for biomedical application. J. Aust. Ceram. Soc. https://doi.org/10.1007/s41779-019-00363-1

Chevalier, E., Chulia, D., Pouget, C., Viana, M., 2008. Fabrication of porous substrates: A review of processes using pore forming agents in the biomaterial field. J. Pharm. Sci. https://doi.org/10.1002/jps.21059

Strens, D., Knerer, G., Van Vlaenderen, I., Dhooge, IJ. 2012. A pilot cost-of-illness study on long-term complications/sequelae of AOM. B-ENT 8, 153–165.

Derakhshanfar, S., Mbeleck, R., Xu, K., Zhang, X., Zhong, W., Xing, M., 2018. 3D bioprinting for biomedical devices and tissue engineering: A review of recent trends and advances. Bioact. Mater. 3, 144–156. https://doi.org/10.1016/j.bioactmat.2017.11.008

Drury, J.L., Dennis, R.G., Mooney, D.J., 2004. The tensile properties of alginate hydrogels. Biomaterials. https://doi.org/10.1016/j.biomaterials.2003.10.002

Elsawy, M.A., Kim, K.H., Park, J.W., Deep, A., 2017. Hydrolytic degradation of polylactic acid (PLA) and its composites. Renew. Sustain. Energy Rev. 79, 1346–1352. https://doi.org/10.1016/j.rser.2017.05.143

Fay, J., Puria, S., Decraemer, W.F., Steele, C., 2005. Three approaches for estimating the elastic modulus of the tympanic membrane. J. Biomech. https://doi.org/10.1016/j.jbiomech.2004.08.022

Fernández-Cervantes, I., Morales, M.A., Agustín-Serrano, R., Cardenas-García, M., Pérez-Luna, P. V., Arroyo-Reyes, B.L., Maldonado-García, A., 2019. Polylactic acid/sodium alginate/hydroxyapatite composite scaffolds with trabecular tissue morphology designed by a bone remodeling model using 3D printing. J. Mater. Sci. 9478–9496. https://doi.org/10.1007/s10853-019-03537-1

Gao, G., Cui, X., 2016. Three-dimensional bioprinting in tissue engineering and regenerative medicine. Biotechnol. Lett. https://doi.org/10.1007/s10529-015-1975-1

Gao, Y., Kong, W., Li, B., Ni, Y., Yuan, T., Guo, L., Lin, H., Fan, H., Fan, Y., Zhang, X., 2018. Fabrication and characterization of collagen-based injectable and self-crosslinkable hydrogels for cell encapsulation. Colloids Surfaces B Biointerfaces. https://doi.org/10.1016/j.colsurfb.2018.04.009

Ghassemifar, R., Redmond, S., Zainuddin, Chirila, T. V., 2010. Advancing towards a tissue-engineered tympanic membrane: Silk fibroin as a substratum for growing human eardrum keratinocytes. J. Biomater. Appl. 24, 591–606. https://doi.org/10.1177/0885328209104289

Gladstone, H.B., Jackler, R.K., Varav, K., 1995. Tympanic membrane wound healing. An overview. Otolaryngol. Clin. North Am.

Grover, C.N., Cameron, R.E., Best, S.M., 2012. Investigating the morphological, mechanical and degradation properties of scaffolds comprising collagen, gelatin and elastin for use in soft tissue engineering. J. Mech. Behav. Biomed. Mater. https://doi.org/10.1016/j.jmbbm.2012.02.028

Guvendiren, M., Molde, J., Soares, R.M.D., Kohn, J., 2016. Designing Biomaterials for 3D Printing. ACS Biomater. Sci. Eng. 2, 1679–1693. https://doi.org/10.1021/acsbiomaterials.6b00121

Hamad, K., Kaseem, M., Yang, H.W., Deri, F., Ko, Y.G., 2015. Properties and medical applications of polylactic acid: A review. Express Polym. Lett. https://doi.org/10.3144/expresspolymlett.2015.42

Henton, D.E., Gruber, P., Lunt, J., Randall, J., 2005. Polylactic Acid Technology: A Review. Nat. Fibers, Biopolym. Biocomposites 48674, 527–578.

Hong, P., Bance, M., Gratzer, P.F., 2013. Repair of tympanic membrane perforation using novel adjuvant therapies: A contemporary review of experimental and tissue engineering studies. Int. J. Pediatr. Otorhinolaryngol. 77, 3–12. https://doi.org/10.1016/j.ijporl.2012.09.022

Hutmacher, D.W., Schantz, J.T., Lam, C.X.F., Tan, K.C., Lim, T.C., 2007. State of the art and future directions of scaffold-based bone engineering from a biomaterials perspective. J. Tissue Eng. Regen. Med. https://doi.org/10.1002/term.24

Ilhan, E., Cesur, S., Guler, E., Topal, F., Albayrak, D., Guncu, M.M., Cam, M.E., Taskin, T., Sasmazel, H.T., Aksu, B., Oktar, F.N., Gunduz, O., 2020. Development of Satureja cuneifolia-loaded sodium alginate/polyethylene glycol scaffolds produced by 3D-printing technology as a diabetic wound dressing material. Int. J. Biol. Macromol.

https://doi.org/10.1016/j.ijbiomac.2020.06.086

Jayakumar, R., Prabaharan, M., Nair, S. V., Tamura, H., 2010. Novel chitin and chitosan nanofibers in biomedical applications. Biotechnol. Adv. https://doi.org/10.1016/j.biotechadv.2009.11.001

Jia, S., Yu, D., Zhu, Y., Wang, Z., Chen, L., Fu, L., 2017. Morphology, crystallization and thermal behaviors of PLA-based composites: Wonderful effects of hybrid GO/PEG via dynamic impregnating. Polymers (Basel). 9. https://doi.org/10.3390/polym9100528

Jian, Y.T., Yang, Y., Tian, T., Stanford, C., Zhang, X.P., Zhao, K., 2015. Effect of pore size and porosity on the biomechanical properties and cytocompatibility of porous NiTi alloys. PLoS One. https://doi.org/10.1371/journal.pone.0128138

Kamthai, S., Magaraphan, R., 2015. Thermal and mechanical properties of polylactic acid (PLA) and bagasse carboxymethyl cellulose (CMC B) composite by adding isosorbide diesters, in: AIP Conference Proceedings. https://doi.org/10.1063/1.4918424

Karageorgiou, V., Kaplan, D.., 2005. Porosity of 3D biomaterial scaffolds and osteogenesis. Biomaterials 26, 5474–5491. https://doi.org/10.1016/j.biomaterials.2005.02.002

Kim, J., Kim, C.H., Park, C.H., Seo, J.N., Kweon, H., Kang, S.W., Lee, K.G., 2010. Comparison of methods for the repair of acute tympanic membrane perforations: Silk patch vs. paper patch. Wound Repair Regen. 18, 132–138. https://doi.org/10.1111/j.1524-475X.2009.00565.x

Kim, J.H., Bae, J.H., Ki, T.L., Choung, P.H., Park, J.S., Seong, J.C., Ae, L.I., Eung, T.L., Choung, Y.H., Chung, J.H., 2009. Development of water-insoluble chitosan patch scaffold to repair traumatic tympanic membrane perforations. J. Biomed. Mater. Res. - Part A 90, 446–455. https://doi.org/10.1002/jbm.a.32119

Kosik-Kozioł, A., Costantini, M., Bolek, T., Szöke, K., Barbetta, A., Brinchmann, J., Święszkowski, W., 2017. PLA short sub-micron fiber reinforcement of 3D bioprinted alginate constructs for cartilage regeneration. Biofabrication. https://doi.org/10.1088/1758-5090/aa90d7

Kozin, E.D., Black, N.L., Cheng, J.T., Cotler, M.J., McKenna, M.J., Lee, D.J., Lewis, J.A., Rosowski, J.J., Remenschneider, A.K., 2016. Design, fabrication, and in vitro testing of novel three-dimensionally printed tympanic membrane grafts. Hear. Res. 340, 191–203. https://doi.org/10.1016/j.heares.2016.03.005

Kuypers, L.C., Decraemer, W.F., Dirckx, J.J.J., 2006. Thickness distribution of fresh and preserved human eardrums measured with confocal microscopy. Otol. Neurotol. https://doi.org/10.1097/01.mao.0000187044.73791.92

Laidlaw, D.W., Costantino, P.D., Govindaraj, S., Hiltzik, D.H., Catalano, P.J., 2001. Tympanic membrane repair with a dermal allograft. Laryngoscope. https://doi.org/10.1097/00005537-200104000-00025

Lim, D.J., 1995. Structure and function of the tympanic membrane: a review. Acta Otorhinolaryngol. Belg.

Loh, Q.L., Choong, C., 2013. Three-Dimensional Scaffolds for Tissue Engineering Applications: Role of Porosity and Pore Size. Tissue Eng. Part B Rev. 19, 485–502. https://doi.org/10.1089/ten.teb.2012.0437

Luo, H., Dai, C., Gan, R.Z., Lu, H., 2009. Measurement of young's modulus of human tympanic membrane at high strain rates. J. Biomech. Eng. https://doi.org/10.1115/1.3118770

Matos, B.D.M., Rocha, V., da Silva, E.J., Moro, F.H., Bottene, A.C., Ribeiro, C.A., dos

Santos Dias, D., Antonio, S.G., do Amaral, A.C., Cruz, S.A., de Oliveira Barud, H.G., Silva Barud, H. da, 2019. Evaluation of commercially available polylactic acid (PLA) filaments for 3D printing applications. J. Therm. Anal. Calorim. 137, 555–562. https://doi.org/10.1007/s10973-018-7967-3

Miles, K.B., Ball, R.L., Matthew, H.W.T., 2016. Chitosan films with improved tensile strength and toughness from N-acetyl-cysteine mediated disulfide bonds. Carbohydr. Polym. https://doi.org/10.1016/j.carbpol.2015.11.052

Murphy, S. V., Atala, A., 2014. 3D bioprinting of tissues and organs. Nat. Biotechnol. https://doi.org/10.1038/nbt.2958

Ouyang, L., Yao, R., Zhao, Y., Sun, W., 2016. Effect of bioink properties on printability and cell viability for 3D bioplotting of embryonic stem cells. Biofabrication. https://doi.org/10.1088/1758-5090/8/3/035020

Patch, W.C., Chung, J.H., Ph, D., Choung, Y., Ph, D., 2010. Tympanic Membrane Regeneration Using. Tissue Eng. Part A 16, 225–232.

Rahman, A., Unge, M. Von, Olivius, P., Dirckx, J., 2007. Healing time , long-term result and effects of stem cell treatment in acute tympanic membrane perforation. https://doi.org/10.1016/j.ijporl.2007.04.005

Rodríguez-Vázquez, M., Vega-Ruiz, B., Ramos-Zúñiga, R., Saldaña-Koppel, D.A., Quiñones-Olvera, L.F., 2015. Chitosan and Its Potential Use as a Scaffold for Tissue Engineering in Regenerative Medicine. Biomed Res. Int. https://doi.org/10.1155/2015/821279

Samanta, H.S., Ray, S.K., 2014. Synthesis, characterization, swelling and drug release behavior of semi-interpenetrating network hydrogels of sodium alginate and polyacrylamide. Carbohydr. Polym. https://doi.org/10.1016/j.carbpol.2013.09.004

Savioli Lopes, M., Jardini, A.L., Maciel Filho, R., 2012. Poly (lactic acid) production for tissue engineering applications. Procedia Eng. 42, 1402–1413. https://doi.org/10.1016/j.proeng.2012.07.534

Tanase, C.E., Spiridon, I., 2014. PLA/chitosan/keratin composites for biomedical applications. Mater. Sci. Eng. C 40, 242–247. https://doi.org/10.1016/j.msec.2014.03.054

Teh, B.M., Marano, R.J., Shen, Y., Friedland, P.L., Dilley, R.J., Atlas, M.D., 2012. Tissue Engineering of the Tympanic Membrane. Tissue Eng. Part B Rev. 19, 116–132. https://doi.org/10.1089/ten.teb.2012.0389

Thomas, M.S., Pillai, P.K.S., Faria, M., Cordeiro, N., Barud, H., Thomas, S., Pothen, L.A., 2018. Electrospun polylactic acid-chitosan composite: a bio-based alternative for inorganic composites for advanced application. J. Mater. Sci. Mater. Med. https://doi.org/10.1007/s10856-018-6146-1

Tighzert, W., Habi, A., Ajji, A., Sadoun, T., Daoud, F.B.O., 2017. Fabrication and characterization of nanofibers based on poly(lactic acid)/chitosan blends by electrospinning and their functionalization with phospholipase A1. Fibers Polym. https://doi.org/10.1007/s12221-017-6953-x

Torres-Hernández, Y.G., Ortega-Díaz, G.M., Téllez-Jurado, L., Castrejón-Jiménez, N.S., Altamirano-Torres, A., García-Pérez, B.E., Balmori-Ramírez, H., 2018. Biological compatibility of a polylactic acid composite reinforced with natural chitosan obtained from shrimp waste. Materials (Basel). https://doi.org/10.3390/ma11081465

Ulag, S., Ilhan, E., Sahin, A., Karademir Yilmaz, B., kalaskar, D.M., Ekren, N., Kilic, O., Nuzhet Oktar, F., Gunduz, O., 2020. 3D printed artificial cornea for corneal stromal

transplantation. Eur. Polym. J. https://doi.org/10.1016/j.eurpolymj.2020.109744

Villar-Fernandez, M.A., Lopez-Escamez, J.A., 2015. Outlook for tissue engineering of the tympanic membrane. Audiol. Res. 5. https://doi.org/10.4081/audiores.2015.117

Wang, D., Hill, D.J.T., Peng, H., Symons, A., Varanasi, S., Whittaker, A.K., Rasoul, F., 2010. Development of injectable biodegradable multi-arms PEG-based hydrogels: Swelling and degradation investigations, in: Macromolecular Symposia. https://doi.org/10.1002/masy.201051033

Weber, D.E., Semaan, M.T., Wasman, J.K., Beane, R., Bonassar, L.J., Megerian, C.A., 2006. Tissue-engineered calcium alginate patches in the repair of chronic chinchilla tympanic membrane perforations. Laryngoscope 116, 700–704. https://doi.org/10.1097/01.mlg.0000208549.44462.fa

Yan, Q., Dong, H., Su, J., Han, J., Song, B., Wei, Q., Shi, Y., 2018. A Review of 3D Printing Technology for Medical Applications. Engineering 4, 729–742. https://doi.org/10.1016/j.eng.2018.07.021

Yang, S., Leong, K.F., Du, Z., Chua, C.K., 2001. The design of scaffolds for use in tissue engineering. Part I. Traditional factors. Tissue Eng. https://doi.org/10.1089/107632701753337645

Yeong, W.Y., Chua, C.K., Leong, K.F., Chandrasekaran, M., Lee, M.W., 2006. Indirect fabrication of collagen scaffold based on inkjet printing technique. Rapid Prototyp. J. https://doi.org/10.1108/13552540610682741

You, F., Wu, X., Chen, X., 2017. 3D printing of porous alginate/gelatin hydrogel scaffolds and their mechanical property characterization. Int. J. Polym. Mater. Polym. Biomater. 66, 299–306. https://doi.org/10.1080/00914037.2016.1201830

Zhang, Q., Lou, Z., 2012. Impact of basic fibroblast growth factor on healing of tympanic membrane perforations due to direct penetrating trauma : a prospective non-blinded / controlled study 446–451.

Zhang, Z., Cui, H., 2012. Biodegradability and biocompatibility study of poly(chitosan-g-lactic acid) scaffolds. Molecules. https://doi.org/10.3390/molecules17033243

Captions for Figures and Tables

Table 1. Content of solutions.

Table 2. Tensile testing results for PLA, 15PLA/3CS, 15PLA/3SA.

Figure 1. Schematic presentation of the 3D printer (a), designing of scaffold on CAD (b), printing process(c), produced scaffold(d), eardrum rapture(e), eardrum patch grafting(f),tympanic membrane regeneration(g).

Figure 2. Viscosity (a,d), Density (b,e) and Surface tension (c,f) of Polylactic acid / Chitosan and Polylactic acid / Sodium alginate solutions.

Figure 3. FTIR spectrums of polylactic acid / chitosan scaffold(a), polylactic acid / sodium alginate scaffold(b).

Figure 4. SEM images and pore size histogram of pure PLA(a), 15PLA/3CS(b), 15PLA/3SA(c) scaffolds, respectively.

Figure 5. DSC thermogram of pure PLA, 15PLA/3CS, and 15PLA/3SA scaffolds.

Figure 6. Swelling(a) and Degradation(b) graphics of pure PLA, 15PLA/3CS, 15PLA/3SA scaffolds.

Figure 7. Cell viability analysis of pure PLA, 15PLA/3CS, 15PLA/3SA scaffolds with their standard deviations (*p<0,05, **p<0,01, ***p<0,001) (A). Fluorescence microscopy images of human mesenchymal stem cells which nucleous stained with DAPI on pure PLA(B-a), 15PLA/3CS(B-b), and 15PLA/3SA(B-c) scaffolds after 7 days incubation (B). SEM images of mesenchymal stem cells on pure PLA(C-a,b), 15PLA/3CS(C-c,d), and 15PLA/3SA(C-e,f) scaffolds (C).

3D printed Scaffold	PLA content (Wt %)	CS content (Wt %)	SA content (Wt %)
15PLA	15	0	0
15PLA/1CS	15	1	0
15PLA/3CS	15	3	0
15PLA/5CS	15	5	0
15PLA/1SA	15	0	1
15PLA/3SA	15	0	3
15PLA/5SA	15	0	5

Table 1

Scaffold	Tensile Strength (MPa)	Elongation at Break (%)
15PLA	14.25	6.41
15PLA/3CS	4.72	4.22
15PLA/3SA	3.51	4.03

Table 2

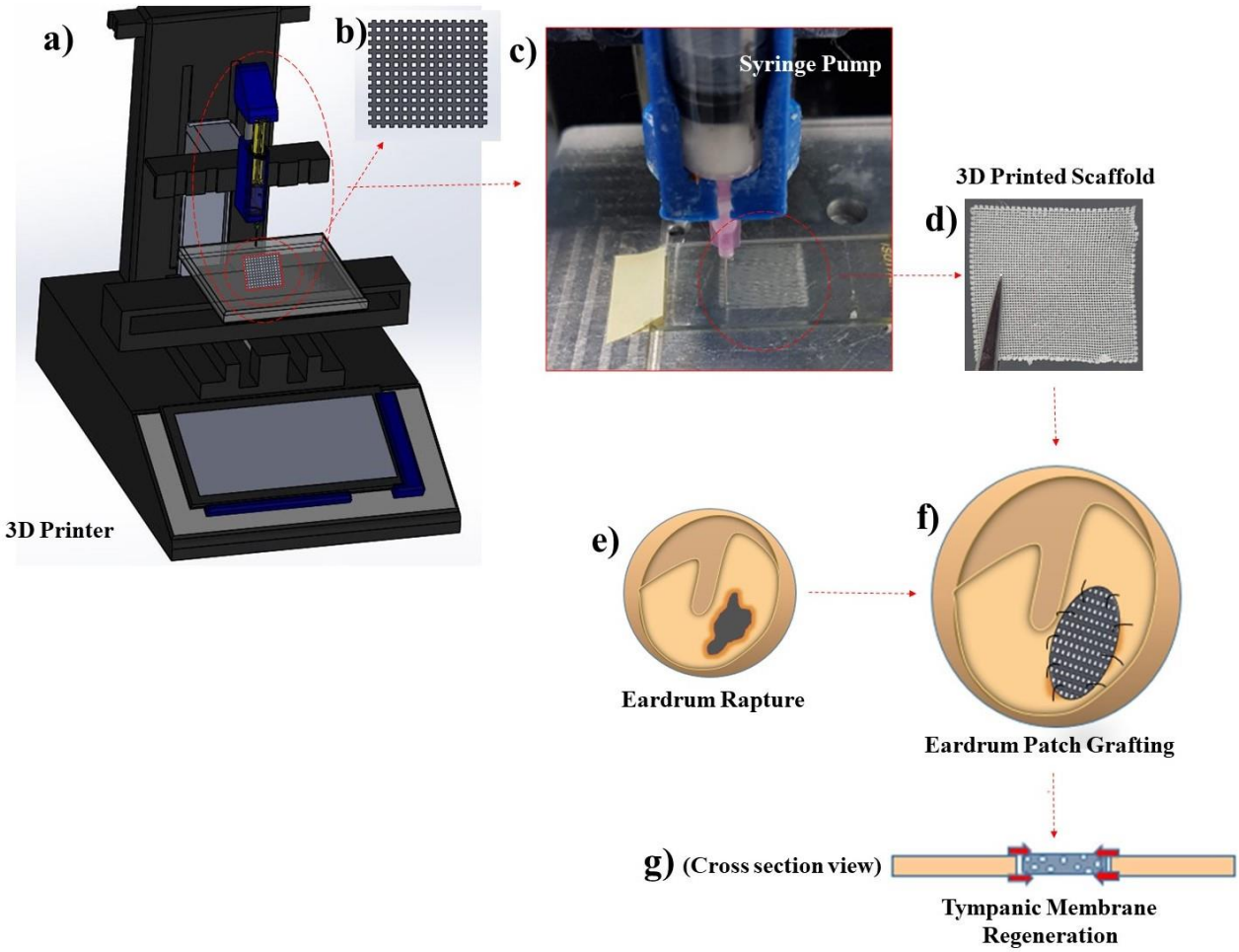
a)
b)
c)
Syringe Pump
3D Printed Scaffold
d)
3D Printer
e)
f)
Eardrum Rapture
Eardrum Patch Grafting
g) (Cross section view)
Tympanic Membrane
Regeneration

Figure 1.

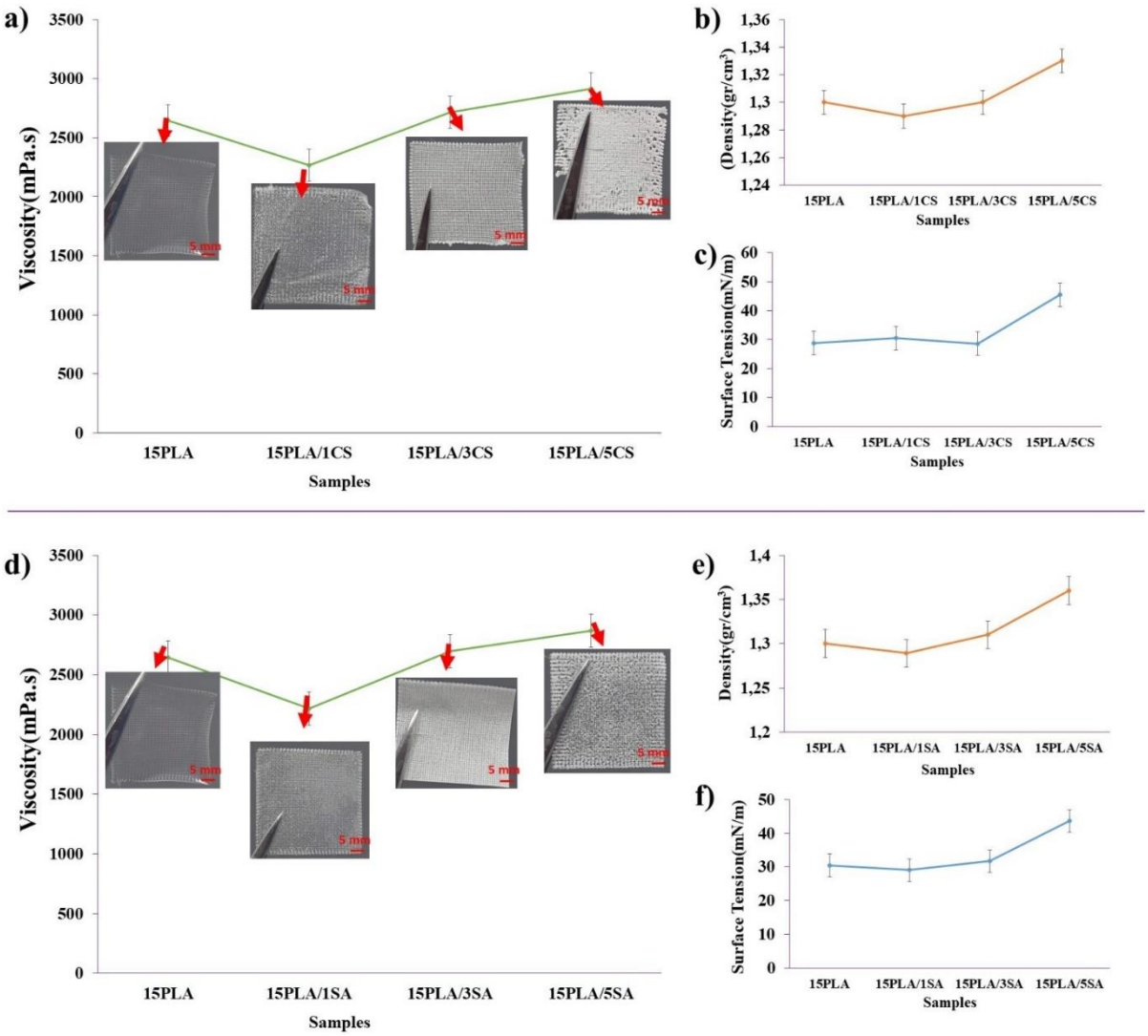
a)
Viscosity(mPa.s)
3500
3000
2500
2000
1500
1000
500
0
15PLA
15PLA/1CS
15PLA/3CS
15PLA/5CS
Samples
5 mm
b)
(Density(gr/cm³)
1,36
1,34
1,32
1,3
1,28
1,26
1,24
15PLA
15PLA/1CS
15PLA/3CS
15PLA/5CS
Samples
c)
Surface Tension(mN/m)
60
50
40
30
20
10
0
15PLA
15PLA/1CS
15PLA/3CS
15PLA/5CS
Samples
d)
Viscosity(mPa.s)
3500
3000
2500
2000
1500
1000
500
0
15PLA
15PLA/1SA
15PLA/3SA
15PLA/5SA
Samples
5 mm
e)
Density(gr/cm³)
1,4
1,35
1,3
1,25
1,2
15PLA
15PLA/1SA
15PLA/3SA
15PLA/5SA
Samples
f)
Surface Tension(mN/m)
50
40
30
20
10
0
15PLA
15PLA/1SA
15PLA/3SA
15PLA/5SA
Samples

Figure 2.

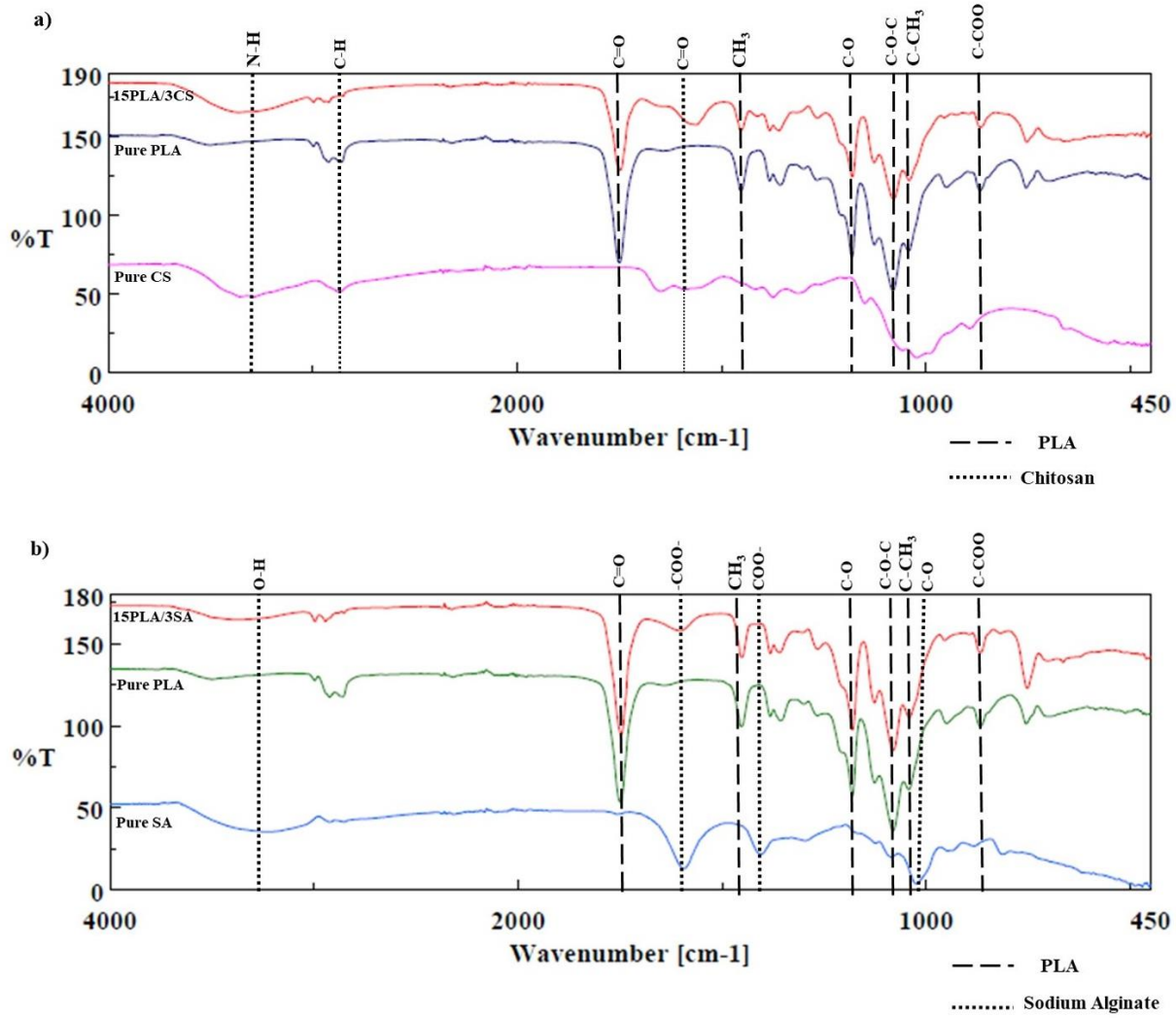
a)
N-H
C-H
C=O
C=O
CH3
C-O
C-O-C
C-CH3
C-COO
190
150
100
50
0
%T
15PLA/3CS
Pure PLA
Pure CS
4000
2000
1000
450
Wavenumber [cm-1]
PLA
Chitosan
b)
O-H
C=O
-COO-
CH3
COO-
C-O
C-O-C
C-CH3
C-O
C-COO
180
150
100
50
0
%T
15PLA/3SA
Pure PLA
Pure SA
4000
2000
1000
450
Wavenumber [cm-1]
PLA
Sodium Alginate

Figure 3.

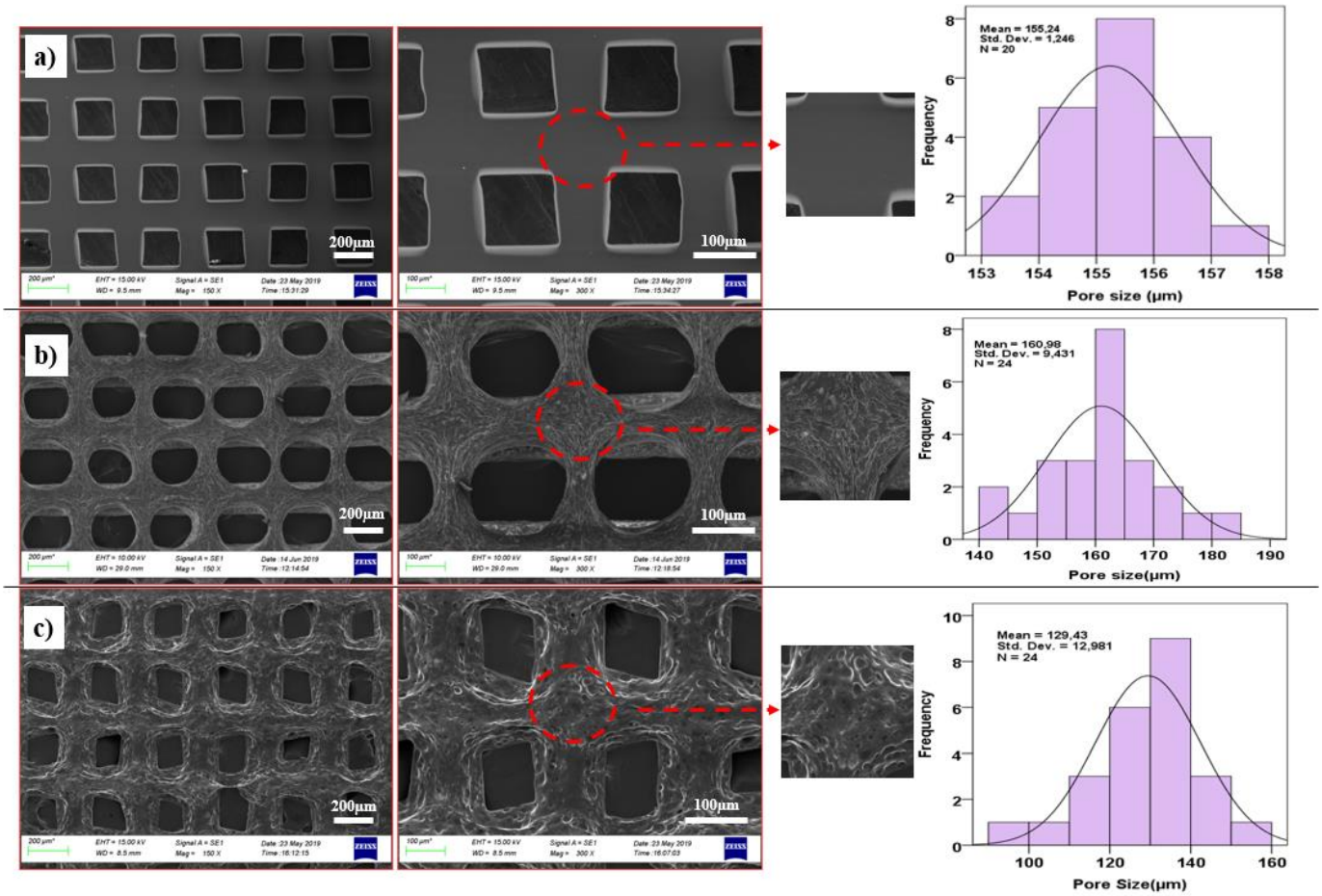
a)
200µm
100µm
Mean = 155,24
Std. Dev. = 1,246
N = 20
Frequency
Pore size (µm)
b)
200µm
100µm
Mean = 160,98
Std. Dev. = 9,431
N = 24
Frequency
Pore size(µm)
c)
200µm
100µm
Mean = 129,43
Std. Dev. = 12,981
N = 24
Frequency
Pore Size(µm)

Figure 4.

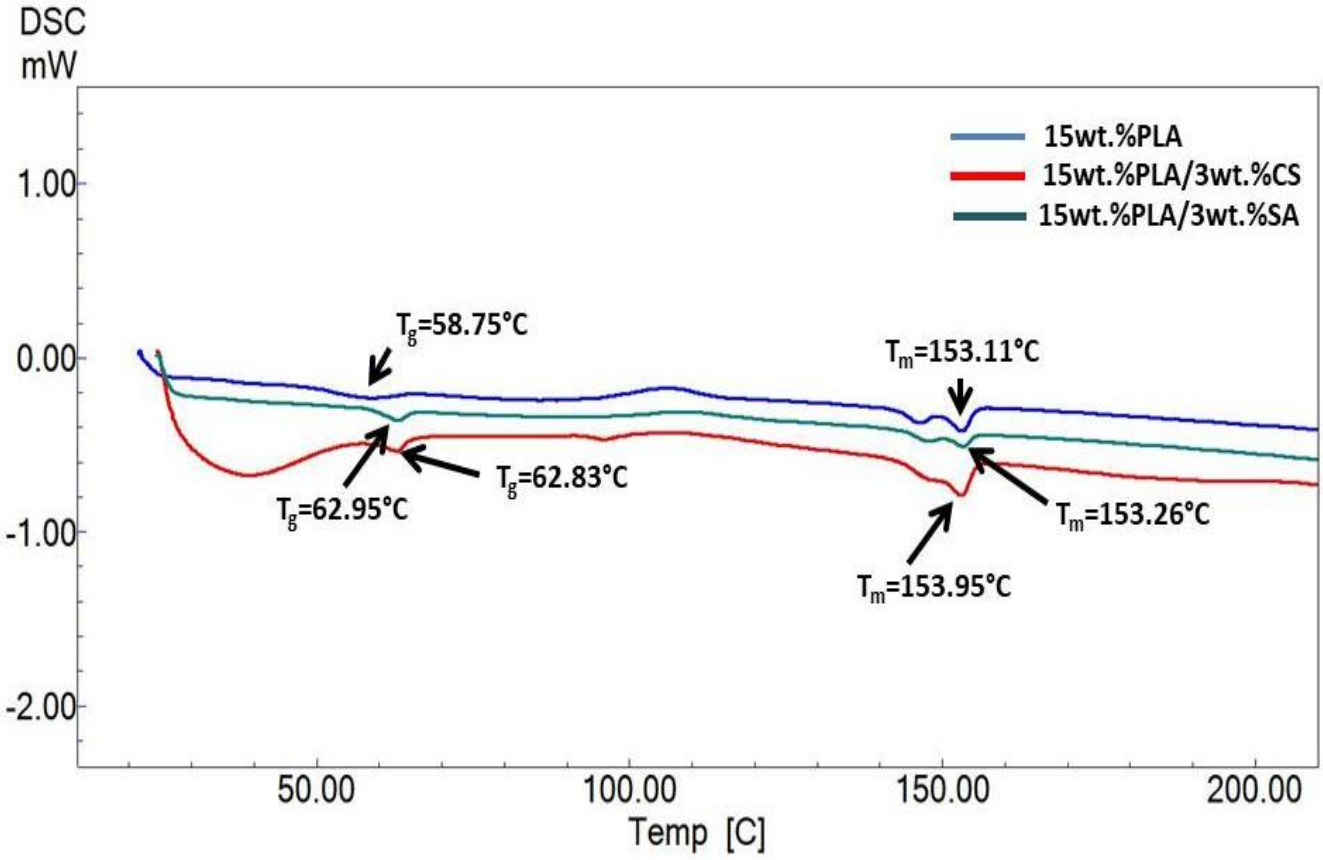
DSC
mW
1.00
0.00
-1.00
-2.00
50.00
100.00
150.00
200.00
Temp [C]
15wt.%PLA
15wt.%PLA/3wt.%CS
15wt.%PLA/3wt.%SA
Tg=58.75°C
Tg=62.95°C
Tg=62.83°C
Tm=153.11°C
Tm=153.26°C
Tm=153.95°C

Figure 5.

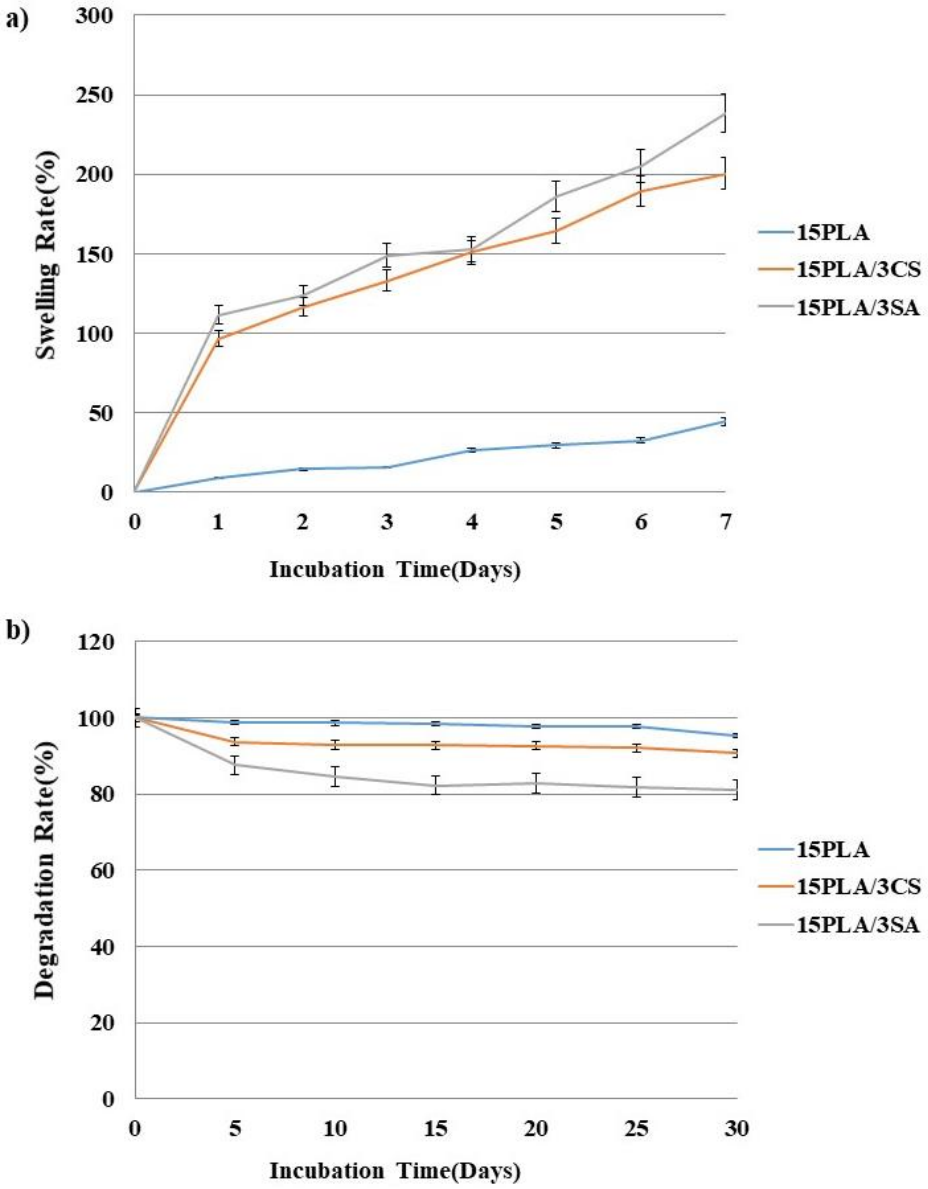
a)
300
250
200
150
100
50
0
Swelling Rate(%)
0
1
2
3
4
5
6
7
Incubation Time(Days)
15PLA
15PLA/3CS
15PLA/3SA
b)
120
100
80
60
40
20
0
Degradation Rate(%)
0
5
10
15
20
25
30
Incubation Time(Days)
15PLA
15PLA/3CS
15PLA/3SA

Figure 6.

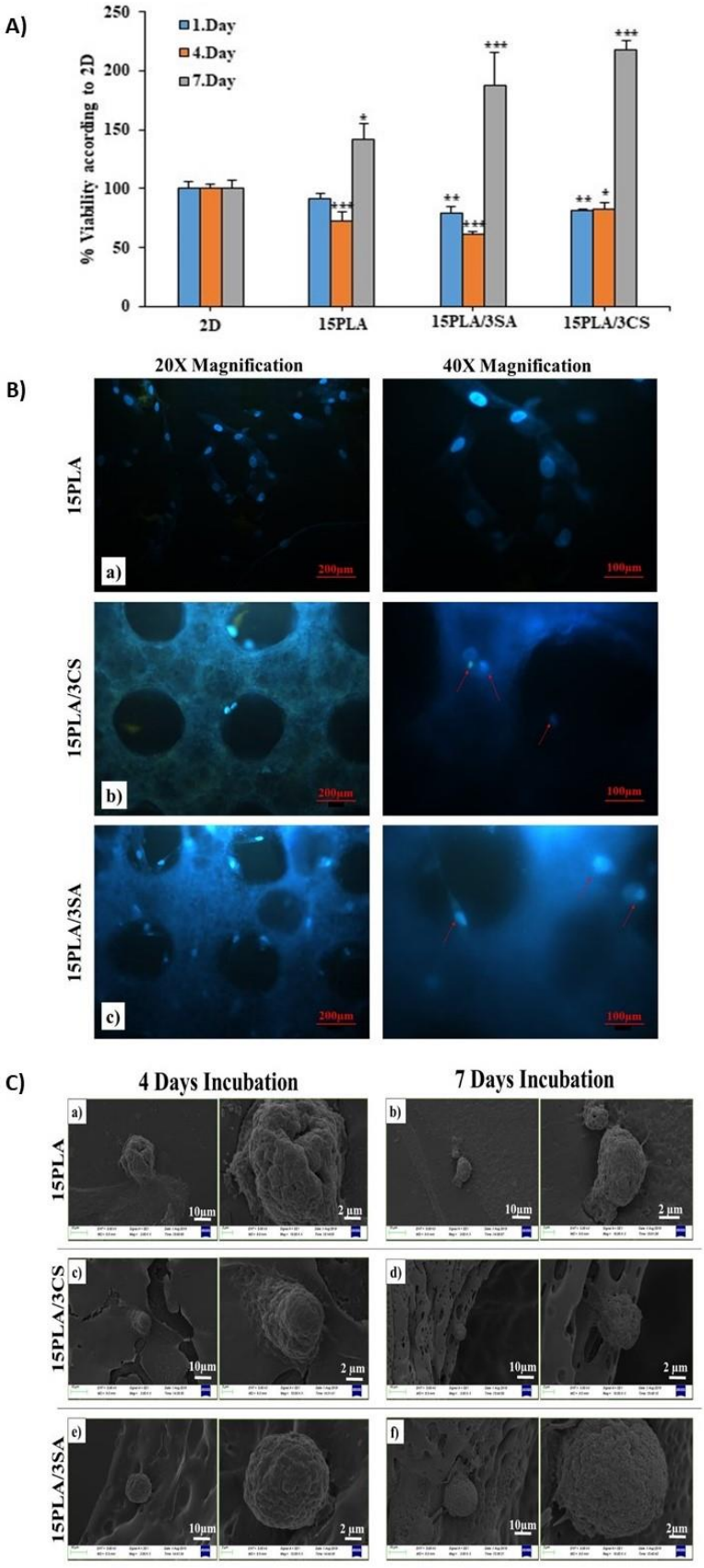
A)
1.Day
4.Day
7.Day
% Viability according to 2D
250
200
150
100
50
0
2D
15PLA
15PLA/3SA
15PLA/3CS
B)
20X Magnification
40X Magnification
15PLA
15PLA/3CS
15PLA/3SA
a)
b)
c)
200µm
100µm
C)
4 Days Incubation
7 Days Incubation
15PLA
15PLA/3CS
15PLA/3SA
a)
b)
c)
d)
e)
f)
10µm
2 µm

Figure 7.